

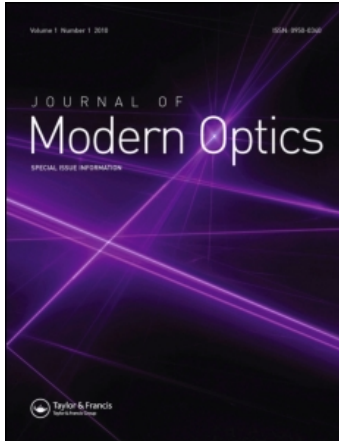
This article was downloaded by:

On: 25 February 2010

Access details: *Access Details: Free Access*

Publisher *Taylor & Francis*

Informa Ltd Registered in England and Wales Registered Number: 1072954 Registered office: Mortimer House, 37-41 Mortimer Street, London W1T 3JH, UK



## Journal of Modern Optics

Publication details, including instructions for authors and subscription information:

<http://www.informaworld.com/smpp/title~content=t713191304>

### Experimental realisation of electromagnetic metamaterials

George Goussetis <sup>a</sup>; Alexandros P. Feresidis <sup>b</sup>; Andrew R. Harvey <sup>c</sup>

<sup>a</sup> Institute for Electronics Communications and Information Technology, Queen's University Belfast, Belfast, UK <sup>b</sup> Department of Electronic and Electrical Engineering, Loughborough University, Loughborough, UK <sup>c</sup> School of Engineering and Physics, Heriot-Watt University, Edinburgh, UK

First published on: 21 January 2010

**To cite this Article** Goussetis, George, Feresidis, Alexandros P. and Harvey, Andrew R.(2010) 'Experimental realisation of electromagnetic metamaterials', *Journal of Modern Optics*, 57: 1, 1 – 16, First published on: 21 January 2010 (iFirst)

**To link to this Article:** DOI: 10.1080/09500340903497515

**URL:** <http://dx.doi.org/10.1080/09500340903497515>

PLEASE SCROLL DOWN FOR ARTICLE

Full terms and conditions of use: <http://www.informaworld.com/terms-and-conditions-of-access.pdf>

This article may be used for research, teaching and private study purposes. Any substantial or systematic reproduction, re-distribution, re-selling, loan or sub-licensing, systematic supply or distribution in any form to anyone is expressly forbidden.

The publisher does not give any warranty express or implied or make any representation that the contents will be complete or accurate or up to date. The accuracy of any instructions, formulae and drug doses should be independently verified with primary sources. The publisher shall not be liable for any loss, actions, claims, proceedings, demand or costs or damages whatsoever or howsoever caused arising directly or indirectly in connection with or arising out of the use of this material.

## TOPICAL REVIEW

### Experimental realisation of electromagnetic metamaterials

George Goussetis<sup>a\*</sup>, Alexandros P. Feresidis<sup>b</sup> and Andrew R. Harvey<sup>c</sup>

<sup>a</sup>Institute for Electronics Communications and Information Technology,  
Queen's University Belfast, Belfast, UK; <sup>b</sup>Department of Electronic and Electrical Engineering,  
Loughborough University, Loughborough, UK; <sup>c</sup>School of Engineering and Physics,  
Heriot-Watt University, Edinburgh, UK

(Received 31 August 2009; final version received 14 November 2009)

By engineering the internal structure of artificial materials it is possible to reproduce effective electromagnetic properties, including some which were previously unavailable in nature. Since the first experimental demonstration of artificial composites with exotic electromagnetic properties at microwaves less than 10 years ago, metamaterials has emerged as a rapidly growing multidisciplinary branch of science and engineering. Significant efforts have been placed in scaling the response of metamaterials to optical frequencies as well as demonstrate pertinent applications of the newly available technology. In this article we review recent developments in the area of experimental realisation of electromagnetic metamaterials and their applications.

**Keywords:** metamaterials; optical composites; artificial electromagnetic materials; medical imaging, MRI

#### 1. Introduction

The electromagnetic characteristics of conventional materials are determined by the interaction of electromagnetic waves with the internal structure of matter, which is typically of a much smaller scale than the wavelength such that materials exhibit the observed bulk values for electric permittivity,  $\epsilon$ , and magnetic permeability,  $\mu$ . There has been considerable recent interest in the development of so-called metamaterials, in which the effective electromagnetic parameters are determined instead by the scattering from structured arrays of subwavelength features. By carefully choosing the geometry of such arrays it is possible to tailor the effective parameters and, significantly, it is possible to provide scattering characteristics that are not found in nature.

Complex engineered media that exhibit customised effective electromagnetic properties have been the topic of research for many decades. An array of subwavelength disks in a periodic arrangement was employed in [1] to produce a convex lens with an effective permittivity. 'Imitated' dielectrics, consisting of periodic arrangements of metallic or dielectric inclusions in a host medium have been investigated in [2] as means to reduce the loss of natural dielectrics at higher frequencies. Isotropic artificial dielectric media composed of a three-dimensional cubic array of metal spheres and dielectric spheres have been investigated

in [3]. In order to improve the mechanical properties, Ward et al. [4] proposed spherical or cylindrical voids in a relatively high dielectric constant base material. Anisotropic dielectrics consisting of finite length of metal strips were studied in [5]. In order to address problems of aerospace research dealing with the interaction of microwave radiation with plasmas, artificial media were proposed in [6] to approximate the behaviour of plasma. In particular, an artificial dielectric composed of periodically spaced lattices of resistive rods was studied and used for implementing a wide range of parameters with medium- and high-loss characteristics [6]. Employing such engineered plasma, in [6] and [7] radiation characteristics from antennas in the presence of plasma were reproduced and the results were in good agreement with established theory.

The interest for artificial media with electromagnetic properties not encountered in natural materials was renewed in the 1990s, mainly by physicists and engineers working on photonic or electromagnetic band gap structures (PBG or EBG) [8] and other engineered periodic structures. In the late 1990s, the realisation of artificial surfaces with properties resembling those of the otherwise non-existent magnetic conductors had been reported and termed artificial magnetic conductors (AMC) or high impedance surfaces (HIS) [9]. In 1999, Pendry et al. [10] proposed that magnetic activity can be obtained from a simple

\*Corresponding author. Email: g.goussetis@hw.ac.uk

array of non-magnetic conducting elements. In particular, it was suggested that arrays of so-called split-ring resonators (SRR), each of those being of subwavelength dimensions, exhibit positive or even negative effective magnetic permeability ( $\mu$ ) when properly excited by plane waves [10]. In the late 1960s, Veselago [11] had already studied theoretically the electromagnetic properties of hypothetical materials in which the permeability and permittivity were simultaneously negative.

The discovery of Pendry in 1999 paved the way for the experimental realisation of artificial materials (meta-materials) with simultaneously negative constitutive parameters ( $\epsilon$  and  $\mu$ ) [12–14]. Since these structures must be much smaller than a wavelength the first manufactured metamaterials were demonstrated at microwave wavelengths where tolerances are readily achieved and metals behave almost as ideal conductors. There is, however, considerable interest in developing metamaterials for use at progressively higher frequencies, ranging initially through THz, infrared and finally optical wavelengths, but this involves considerable challenges. In particular the need for subwavelength internal structure in metamaterials poses the requirement to manufacture structures in the nanometer scale. Moreover, at optical frequencies, metals deviate significantly from ideal conductors, so that direct scaling of the dimensions is not always possible. Nevertheless, the features of optical metamaterials suggest that their manufacture will lead to widespread use in many practical applications, including subwavelength imaging and optical cloaking.

In this article we review recent work in the area of experimental realisation of electromagnetic metamaterials, with emphasis on optical and near-optical frequencies. The article is structured as follows. An overview of experimental realisations of metamaterials that exhibit magnetic activity are discussed in Section 2. Section 3 presents an overview of metamaterials that produce an effective negative index of refraction, while Section 4 discusses some recent realisations of metamaterials with extreme effective parameters, such as extreme anisotropy and near zero permittivity. The two following sections discuss recent demonstrations of applications of metamaterials in superlenses (Section 5), that can resolve images beyond the diffraction limit, and optical cloaking (Section 6). Section 7 discusses the efforts for active metamaterials. An overview of recent work on planar metamaterials (metasurfaces) and their emerging applications is given in Section 8. Section 9 is dedicated to experimental investigations on the applications of metamaterials in medical imaging.

## 2. Magnetic response

Following the prediction of the magnetic response from split-ring resonators [10], such structures were successfully realised in the microwave regime [12]. Shortly after, research efforts were focused on producing magnetic response at higher frequencies by scaling the physical dimensions of the split-ring resonators and today they are available across the spectrum up to, and including, the visible.

In [15], magnetic response was reported for 2D periodic planar arrays of concentric split-ring resonators in the range of 1 THz. The metallic array was formed by 3  $\mu\text{m}$  thick copper on 400  $\mu\text{m}$  thick quartz substrate using a photo-proliferated process [15]. To characterise a planar array, free-space characterisation for an oblique linearly polarised incidence was undertaken. In particular, an obliquely incidence transverse electric wave was employed, since an oscillating magnetic field perpendicular to the plane of the split-ring resonator is required for magnetic excitation of the array.

Stretching the frequency by two orders of magnitude, Enkrich et al. [16] demonstrated experimentally a magnetic resonance response at 100 THz using nano-fabricated gold SRR-like elements arranged in periodic quadratic arrays. This frequency was doubled in [17] where a structure of 50 nm minimum feature size ‘u’-shaped 30 nm thick gold split-ring resonators on 1 mm glass substrate was experimentally tested. These structures were fabricated using electron beam lithography. In [17], a higher order magnetic resonance is reported, pushing the frequency of magnetic responses with split-ring resonators to 370 THz (wavelength of 800 nm).

A non-planar variant consisting of a 1D and 2D periodic array of gold ‘staples’ each with two outwardly splayed footings was reported in [18] to produce a magnetic response at around 60 THz (mid-infrared). These arrays were fabricated in gold on a zinc sulfate substrate using interferometric lithography on photo-resist and reactive ion etching. A thick solid layer of gold was deposited as a ground plane, so that the arrays could only be tested in the reflection mode. A periodic system composed of five layers of split-ring resonators exhibiting magnetic resonance at around 6 THz was reported in [19]. The metallic arrays, with unit cell 7  $\mu\text{m}$  were fabricated in silver and photolithographically aligned with an accuracy of the order of 0.5  $\mu\text{m}$ . The structure was fabricated in a layer-by-layer fashion alternating 5  $\mu\text{m}$ -thick slabs of polyimide spun on 1  $\mu\text{m}$ -thick silver films, which are deposited and patterned using standard lift-off techniques.

In [20,21], it is argued that the scaling of split-ring resonators to produce magnetic response at

increasingly higher frequency has an upper frequency limit. This can be seen by the following argument; the energy that has to be pumped into a coil in order to support current  $I$  is equal to the magnetic energy stored ( $\frac{1}{2}LI^2$ ). In addition to that, the kinetic energy of the charge carriers needs to be considered. For an ideal conductor with infinite carrier density, the carrier velocity and kinetic energy is zero. However, for a real metal with finite carrier density, the carrier velocity and kinetic energy is non-zero even for finite current flow. The carrier kinetic energy can be expressed as an effective additional magnetic energy with an equivalent inductance,  $L_{\text{kin}}$ , which adds to the coil inductance:  $L \rightarrow L + L_{\text{kin}}$ . The kinetic inductance,  $L_{\text{kin}}$ , is negligible for large coil inductances,  $L$ , but becomes dominant for small coils. Therefore, in the limit of small split-ring resonators, the resonant frequency becomes independent of the size [20,21]. In [21] magnetic metamaterials composed of 35 nm minimum feature-size gold split-ring resonators with a fundamental magnetic resonance at a wavelength of 900 nm were presented (Figure 1). More exact calculations undertaken using the complex dielectric function of metals as determined from experiments in the literature have demonstrated that the practical limit of scaling split-ring resonators to achieve magnetic response are to be found at around this wavelength, setting the highest frequency of magnetic response with split-ring resonators to date at 800 nm [17].

This limitation together with the technological challenge to form a bulk 3D metamaterial structure in the nanometer scale suggested the requirement for alternative designs suitable for the visible range.

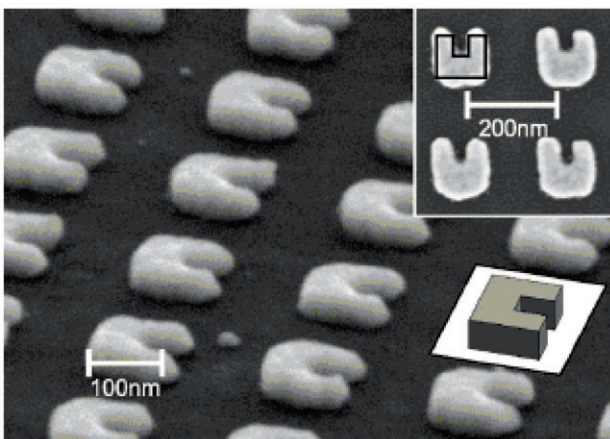


Figure 1. Electron micrograph of the gold split-ring resonator array reported in [21] exhibiting magnetic resonance at 900 nm. The inset shows a top-view image in the same scale [21]. Reprinted with permission from Klein et al., *Opt. Lett.* 2005, 31, 1259–1261. Copyright (2005) by Optical Society of America. (The colour version of this figure is included in the online version of the journal.)

The key idea that emerged was based on pairs of metal wires or metal plates, fabricated on either side of a dielectric spacer [22]. Theoretical studies have shown that a magnetic resonance with antiparallel currents can be established in a pair of coupled nanorods or nanostrips, which can in turn provide an effective diamagnetic or paramagnetic response.

Extending the work in [23] for red light, a series of prototypes involving coupled nanostrips with varying dimensions have been tested and demonstrated to produce a magnetic response across the visible spectrum [24]. The samples were fabricated by electron beam lithography techniques on glass substrates. Electron beam deposition was used to produce a stack of silver and alumina layers and the paired strip structures were obtained after a lift-off process. A series of six samples with different dimensions were produced. Distinct colours in different samples both in transmission mode and reflection mode were observed (reproduced in Figure 2) for the resonant TM polarisation incidence (while the same colours were observed for the non-resonant TE incidence) [24]. In particular, and as theoretically predicted, the position of the magnetic resonance moves towards shorter wavelengths as the width of the nanostrip pair decreases.

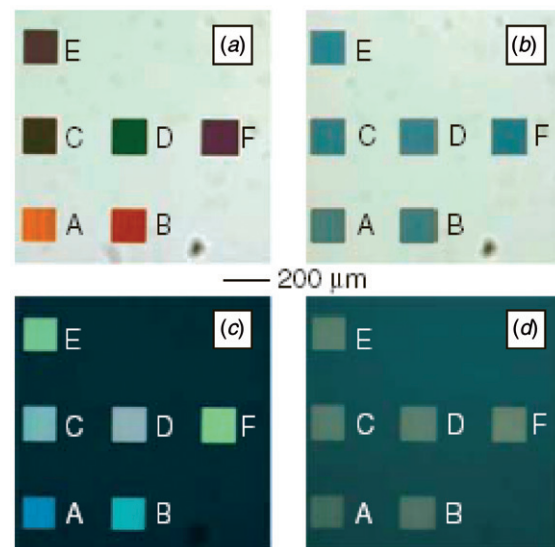


Figure 2. Optical microscope image of magnetic arrays consisting of paired nanorods for the two orthogonal polarisations. The size of each sample is  $160 \mu\text{m} \times 160 \mu\text{m}$ . (a) Transmission mode with TM polarisation, (b) transmission mode with TE polarisation, (c) reflection mode with TM polarisation, and (d) reflection mode with TE polarisation [24]. Reproduced with permission from Cai et al., *Opt. Express* 2007, 15, 3333–3341. Copyright (2007) by Optical Society of America. (The colour version of this figure is included in the online version of the journal.)

### 3. Negative refraction

Negative-index metamaterials (NIMs) were first realised and demonstrated at microwave frequencies [12] following Pendry's discovery of magnetic response from arrays of SRRs in 1999. A bulk structure consisting of an array of strip wires to synthesise a negative permittivity and SRRs (or capacitively loaded loops) to synthesise negative permeability was assembled. By measuring the scattering angle from a prism fabricated from this material (Figure 3(a)) a negative refractive index was experimentally verified for the first time (Figure 3(b)).

Comprehensive recent comparative reviews on the realisation of metamaterials with negative index of refraction can be found in [25–28]. A variant structure of the original shown in [12] where the split rings are substituted by pairs of short coupled wires was demonstrated to produce an effective negative refraction for a linearly polarised incident wave at about 14 GHz [29]. Another variant structure consisting of periodic arrays of 'H'-shaped metallic wires was demonstrated to produce a similar effect at about 16 GHz [30]. An impedance-matched, metamaterial consisting of split-ring resonators and tuned electric resonators instead of wires was presented in [31] to produce negative index of refraction at around 10 GHz.

A bulk metamaterial composite based on split-ring resonators and micron-scale metallic wires is reported in [32]. The unit cell of the metamaterial reported in [32] contains two coplanar concentric split-ring resonators, and two layers of triple wire pattern. The patterns were fabricated in gold and on glass substrates using UV photolithography and the bulk metamaterial consisted of ten unit cells in the propagation direction. One hundred such layers were assembled so that the bulk crystal was 15 mm wide. The transmission

spectrum shows a transmission at around 100 GHz. Theoretical studies by the authors associated this passband with a negative index of refraction [32].

#### 3.1. Paired nanorods

As frequencies increase, the magnetic response of the split-ring resonator saturates and therefore split-ring resonators cannot be used to scale negative refractive index metamaterials to optical frequencies. Instead the coupled nanorod or nanostrip pair produces magnetism at optical frequencies with equivalent negative values for the effective magnetic permeability (i.e.  $\mu < 0$ ) at certain frequencies. A schematic representation is shown in Figure 4. Moreover, the excitation of resonant current oscillation in the strips can produce an effective negative electric permittivity (i.e.  $\varepsilon < 0$ ). If the frequencies where  $\mu < 0$  and  $\varepsilon < 0$  overlap, then an effective negative index of refraction is achieved [33].

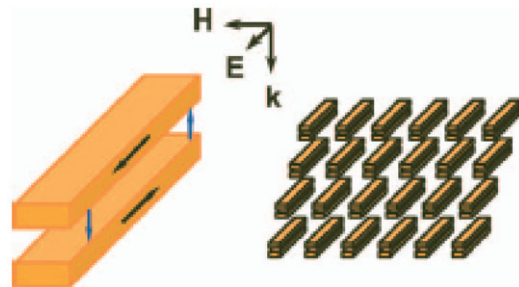


Figure 4. Schematic representation of a coupled nanorods array [34]. Reproduced with permission from Shalaev et al., *Opt. Lett.* 2005, 30, 3356. Copyright (2005) by Optical Society of America. (The colour version of this figure is included in the online version of the journal.)

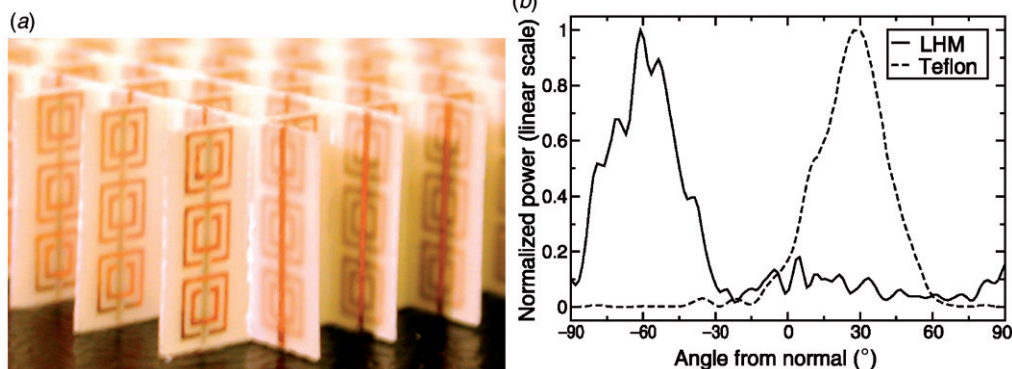


Figure 3. (a) Photograph of the first NIM [12]. (b) Transmitted power at 10.5 GHz as a function of refraction angle for both a Teflon sample (dashed curve) and a LHM sample (solid curve). The two curves were normalised such that the magnitude of both peaks is unity [12]. Reprinted with permission from Shelby et al., *Science* 2001, 292, 77. Copyright (2001) by AAAS. (The colour version of this figure is included in the online version of the journal.)

An experimental demonstration of paired gold nanorods exhibiting negative index of refraction at near infrared, is reported in [34] and simultaneously in [35]. In [34] the thickness of the rods was 50 nm and a silicon dioxide layer of thickness 50 nm was used as a spacer. The fabrication procedure resulted in a trapezoidal shape of the rods with the dimension of the bottom rods  $780\text{ nm} \times 220\text{ nm}$  and the top rods  $670\text{ nm} \times 120\text{ nm}$ . Numerical and experimental results in agreement demonstrated an effective negative refractive index of about  $n = -0.2$  at the telecommunication wavelength of  $1.5\text{ }\mu\text{m}$ . In [35] rods or cut-wires of 20 nm thickness were used on either side of a  $\text{MgF}_2$  substrate. Furthermore, their width was increased until it was equal to the length resulting in nanoscopic square plate pairs, with transmission/reflection responses independent of the incident polarisation, a feature desirable for applications such as perfect lenses.

### 3.2. Fishnet structure

Despite the successful demonstration of negative index of refraction at optical frequencies in [34], it is normally difficult to arrange for the electric permittivity and magnetic permeability to be simultaneously negative [36]. An alternative design which combines the magnetic coupled strips (that yield  $\mu < 0$ ) with continuous electric strips (that yield  $\epsilon < 0$ ) in a broad spectrum is the so-called fishnet structure. The operation is summarised in Figure 5.

An experimental demonstration of a negative index material with such a ‘fishnet’ structure at mid-infrared

is reported in [37]. The metamaterial structure consists of two gold fishnet arrays of thickness 30 nm separated by a 60 nm thick spacer of alumina. The holes were of diameter 360 nm at a pitch of 838 nm. The metamaterial array was tested in a Fourier-transform infrared (FTIR) spectrometer, where the phase information of the reflection and the transmission was obtained using phase masks and an interferometric arrangement. The geometrical symmetry of the structure, which had a square unit cell, made the metamaterial almost insensitive to the polarisation of the incoming light, enabling unpolarised light to be used for testing. An effective index of refraction of around  $n = -3$  was reported at a wavelength of about  $2\text{ }\mu\text{m}$ .

A metamaterial that exhibits negative index of refraction of  $n = -2$  at around  $1.45\text{ }\mu\text{m}$  wavelength and low thermal losses is reported in [38]. In order to quantify the losses, the figure of merit is defined as the negative ratio of the real part of the effective refractive index, divided by the imaginary part. The figure of merit was optimised employing low-loss materials (e.g. silver as metal) and tuning the wire widths as well as the metal and spacer thickness, of the design. The optimisation introduces a dependence of the final design on the metal (silver) plasma frequency and the incident polarisation (the structure in [38] produces an effective negative index of refraction for a specific linear polarisation). The maximum figure of merit was about 3 at a wavelength where the real part of the refractive index is about  $n = -1$ . For comparison, the authors report that the figure of merit was about 0.1 and less than 1 in [34] and [37], respectively.

In [39] a metamaterial that has a negative index of refraction at  $1.5\text{ }\mu\text{m}$  is reported to produce simultaneous negative phase and group velocity. Using standard electron-beam lithography and electron-beam evaporation, a series of fishnet structures were fabricated. The metallic arrays were made from gold and  $\text{MgF}_2$  was used for a spacer. Employing a Michelson interferometer arrangement with and without the sample, the authors extracted the phase time delay and from the shift of the pulse-envelope the group delay was determined. Within a wavelength range, simultaneous phase and group velocity were reported, suggesting that the pulse envelope peak appears at the rear end of the sample before the input pulse has entered the front side. To further improve the losses and reduce the operating wavelength, the metallic arrays were fabricated in silver in [40] with  $\text{MgF}_2$  used as spacer. The total thickness of the sample reported in [40] is 97 nm and the lattice constant 300 nm. A similar experimental setup as in [39] was employed within the wavelength range 700 to 1500 nm. An index of refraction of about  $n = -0.6$  is reported at wavelength 780 nm with a figure of merit of about 0.5.

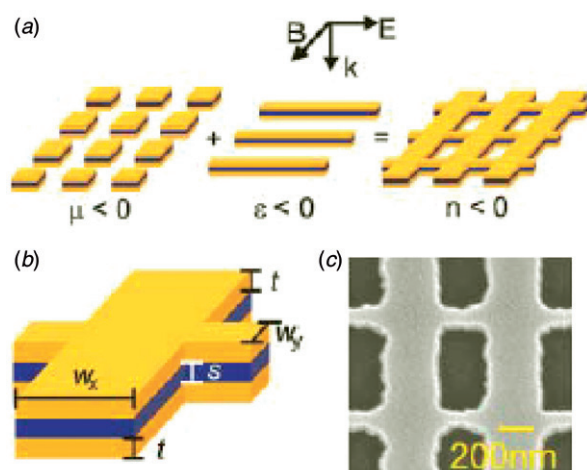


Figure 5. Scheme for the fishnet metamaterial with negative index of refraction.  $\mathbf{E}$  and  $\mathbf{B}$  are the vectors of the incident electric and magnetic field and  $\mathbf{k}$  the incident wavevector [39]. Reprinted with permission from Dolling et al., *Science* 2006, 32, 892–894. Copyright (2006) by AAAS. (The colour version of this figure is included in the online version of the journal.)

A metamaterial with negative index of refraction at wavelength 810 nm was reported in [41]. Using electron-beam lithography followed by electron-beam evaporation and lift-off, a metamaterial consisting of two 33 nm layers of periodically perforated silver (fishnet) separated by 28 nm of alumina was fabricated. The period of the structure is 300 nm. This metamaterial produces two bands of negative index of refraction between wavelengths of 799 to 818 nm and 753 to 810 nm, respectively, for two orthogonal linear polarisations, respectively. The former band yields negative values for both electric permittivity and permeability (therefore termed as double negative), while the latter yields a negative value only for the electric permittivity (and positive for the magnetic permeability). However, the necessary condition for producing an effective negative index of refraction,  $\epsilon'\mu'' + \epsilon''\mu' < 0$  where  $\epsilon''$  and  $\mu''$  correspond to the real and imaginary part of the electric permittivity and magnetic permeability, respectively (see [41] and references therein), is satisfied in both bands. The best figure of merit reported was 1.3 and obtained at wavelength 813 nm, where the refractive index (real part) is approximately equal to  $-1$ . The minimum value of the refractive index obtained at wavelength 820 nm was  $-1.3$  with a figure of merit of 0.9. Within the 799 to 818 nm wavelength range, the index of refraction varied within the range  $-1.2 \pm 0.1$ . For the other polarisation (wavelength band 753 to 810 nm), the best figure of merit was 0.7 and obtained at a wavelength of 772 nm where the index of refraction is approximately  $n = -0.9$ . The lowest index of refraction in this band was  $n = -1$  at wavelength 776 nm.

In [27] and references therein, a dual-band metamaterial structure with response blue-shifted compared to [41] is reported. The metamaterial, fabricated in a similar manner as in [41], produced a dual-band response (dual and single negative) for the two orthogonal polarisations between about 720 to 730 nm and 660 to 810 nm, respectively. Within the former band (dual negative), the maximum value for the figure of merit is equal to 1.05 at wavelength of 725 nm, where the refractive index was about  $n = -0.8$ . The minimum value of the refractive index was  $n = -1.2$  at wavelength 735 nm and figure of merit 0.7. For the single negative band, the minimum index of refraction was approximately  $n \approx -0.5$  at wavelength 710 nm and a figure of merit approximately equal to 0.5.

A 3D metamaterial consisting of cascaded fishnet structures with negative index of refraction at wavelengths in the range of about 1500 nm to beyond 1800 nm for a specific linear polarisation is reported in [42] (Figure 6(a)). The metamaterial was fabricated on

a multilayer metalo-dielectric stack using focused ion-beam milling, which is suitable to cut features of the order of nanometers with a high aspect ratio. A device milled on 21 alternating films of silver and magnesium fluoride producing 10 functional layers has been fabricated and tested. The authors report that the refractive index obtained remains consistent for fishnet metamaterials with three or more functional layers. In order to measure the index of refraction, the authors of [42] also fabricated two prisms made of the metamaterials with angles  $5^\circ$  and  $4.7^\circ$  and experimentally demonstrated negative refraction of an incoming linearly polarised incident beam (Figure 6(b)). By measuring the beam shifting of the light after the prism, the authors directly extracted the index of refraction for wavelengths between 1200 and 1800 nm (Figure 6(c)). For shorter wavelengths, the beam refracts in the positive direction, suggesting a positive value of the refractive index. At 1475 nm, the index of refraction was found to approach zero. Beyond that frequency, the beam was refracting in the negative direction [42]. The refractive index varied from about  $n = 0.63$  at wavelength of 1200 nm to about  $n = -1.23$  at wavelength of 1775 nm. The figure of merit was estimated from the transmission and reflection of normally incident polarised light on the 21 layer structure. A measured value for the figure of merit of about 3.5 at a wavelength of 1775 nm where the refractive index is  $n = 1.23$  is reported.

### 3.3. Chirality

An alternative route to negative refraction was proposed in [43] (and then in [44] and [45]) and involves the use of material chirality. A chiral material lacks planes of mirror symmetry and electromagnetically is characterised by coupling between the electric and magnetic dipoles along the same direction. As a consequence, the degeneracy between the two circular polarisations is broken and the index of refraction is higher for one circular polarisation than the other. Thus a strongly chiral medium is possible to exhibit negative index of refraction for one polarisation and positive for the other.

An experimental indication as a signature of negative refraction due to chirality was reported in [46], although the transmission levels were very low. A recent paper [47] reported a further experimental demonstration of chirality-induced negative index of refraction at microwave frequencies, although the transmission levels were still low. Negative values for the effective electric permittivity,  $\epsilon$ , and magnetic permeability,  $\mu$ , as well as refractive index,  $n$ , were obtained by measurements in a series of samples.

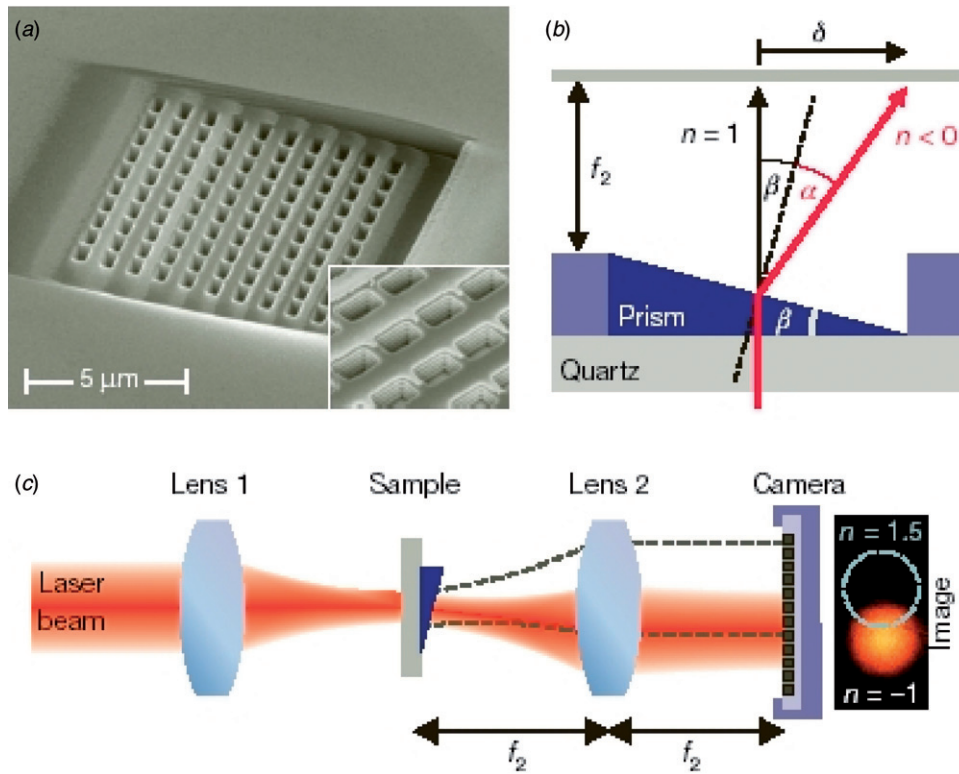


Figure 6. (a) Scan electron microscope image of a 3D fishnet prism and magnified view with the film layers visible in each hole (inset). (b) Schematic of the experimental setup involving the 3D fishnet prism. By measuring  $\delta$  the absolute angle of refraction,  $\alpha$ , can be obtained. (c) Schematic of the experimental setup for the refraction measurement [42]. Reprinted with permission from Valentine et al., *Nature* 2008, 455, 376–379. Copyright (2008) by Nature Publishing Group. (The colour version of this figure is included in the online version of the journal.)

The authors suggest that the negative value of the index of refraction  $n = (\epsilon\mu)^{1/2} \pm \kappa$  originates not from the negative values of the  $\epsilon$  and  $\mu$ , but rather from the large contribution of the chirality parameter,  $\kappa$ . An experimentally observed value of  $n = -1.7$  at about 4.5 GHz with a figure of merit equal to 0.5 are reported for right-handed circular polarisation and a sample made on FR4 substrate.

A chiral metamaterial exhibiting opposite signs for the effective refractive indices of the two circularly polarised waves around 1 THz has been recently reported in [48]. The design was based on a vertical metallic (gold) chiral resonator, where the chirality is introduced by tilting the loop out of the plane with its gap (Figure 7). The loop forms an equivalent inductor, while the two bottom strips form a capacitor. The resonator can be excited by either an electric field across the gap or a magnetic field normal to the loop. Therefore strong electric and magnetic responses can be generated and the structure can be considered as a combination of an electric and a magnetic dipole moment [48]. Samples of 1.5 cm by 1.5 cm were fabricated and the transmission and reflectance were

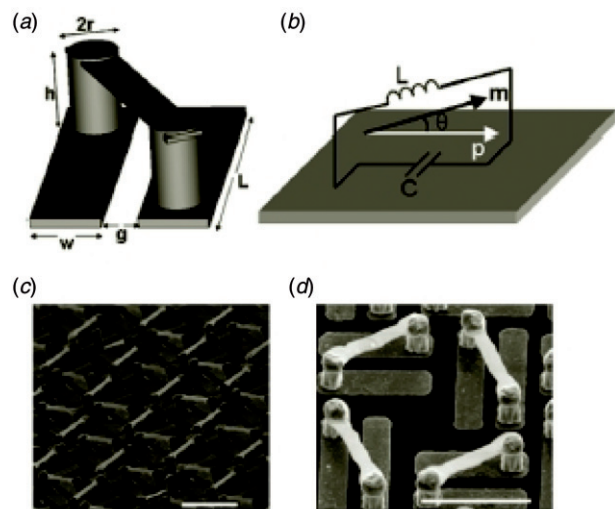


Figure 7. (a) Schematic of the chiral structure proposed in [48] and (b) equivalent circuit. Parts (c) and (d) are scan electron microscope images of the fabricated samples in [48]. Reprinted figure with permission from Zhang et al., *Phys. Rev. Lett.* 2009, 102, 023901. Copyright (2009) by the American Physical Society. (The colour version of this figure is included in the online version of the journal.)

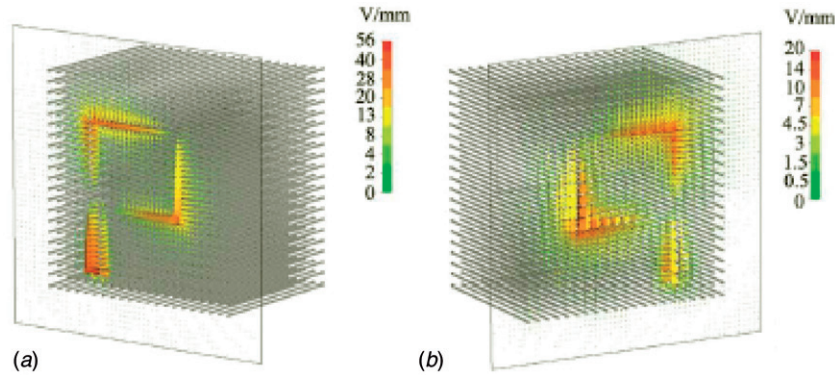


Figure 8. Distribution of the electric fields in the source (a) and image (b) plane for the wire medium lens reported in [49,50]. Reprinted figure with permission from Belov et al., *Phys. Rev. B*. 2006, 73, 033108. Copyright (2006) by the American Physical Society. (The colour version of this figure is included in the online version of the journal.)

measured using THz time-domain spectroscopy for the two linear orthogonal polarisations. Extracting the transmission of left and right circularly polarised waves from these measurements, the authors demonstrated negative values for the refractive index of left-handed waves in the frequency range between 1.06 and 1.27 THz, with a minimum index below  $-5$ . As in [46,47], the transmission levels in this case were low. For the right-handed polarisation, the refractive index was positive over the whole frequency range.

#### 4. Extreme effective parameters

Materials with extreme parameters or extreme properties, such as near zero permittivity, extreme anisotropy, or very large permittivity, may also have a number of interesting applications. A highly anisotropic magnetic metamaterial consisting of an array of ‘swiss rolls’, which act as magnetic wires, was demonstrated in [49] to transfer an input magnetic field pattern with a spatial resolution equal to the roll diameter. An array of 271 individually tuned rolls of about 10 mm each was assembled and demonstrated to transfer the magnetic flux produced by a pair of anti-parallel wires in the shape of the letter M to a distance of about 70 mm at 21.3 MHz [49]. The peak value of the permeability reported for the swiss rolls in [49] was about 35 and the quality factor was about 60.

Transfer of images with subwavelength resolution has also been demonstrated by an array of parallel conducting wires exhibiting strong spatial dispersion [50] (Figure 8). Operating in the canalisation regime, the subwavelength resolution is not based on a resonant effect, offering 18% bandwidth for a  $\lambda/15$  resolution. Although to a certain extent this is an electrical equivalent of [49], the magnetic wires formed by the swiss rolls are resonant and therefore inherently narrowband and lossy. In contrast, the low losses due

to the non-resonant operation of the lens in the canalisation regime allows for transmitting a sub-wavelength image at large distances without significant distortion [51]. The bandwidth of a wire medium lens is determined by the matching condition, which requires a Fabry–Pérot resonance to be formed along the length of the lens.

Recently experimental observation of negative refraction in a bulk metamaterial consisting of closely spaced nanowires has been reported [52]. The sample was prepared by electrochemical deposition of silver nanowires in a porous alumina template formed by electrochemical anodisation. The sample was illuminated by a polarised diode laser beam at different angles through a slit of  $1\ \mu\text{m}$  etched through a 250 nm thick silver coating film [52] and the transmitted light was mapped by scanning an optical fibre at the other end. As a result of the hyperbolic dispersion of the nanowire medium, incoming transverse magnetic polarised beams at wavelength of 660 nm and 780 nm underwent negative refraction (despite the fact that the phase velocity remained positive). In particular the group refractive index was found to be  $-4$  for this polarisation at 780 nm, while the phase refractive index was positive. In contrast, transverse electric waves underwent positive refraction. Calculations by the authors in [52] suggest that negative refraction occurs also for longer wavelength. Moreover, the light intensity at normal incidence was measured to decay by about  $0.43\ \mu\text{m}^{-1}$ , a loss that corresponds to a few orders of magnitude lower than that of the single layer metamaterial reported in [53]. The broad bandwidth and low loss characteristics are in accordance with the non-resonant operation of the wire medium.

Energy squeezing and tunneling through an ultra-narrow waveguide channel that mimics epsilon near zero (ENZ) permittivity properties was experimentally demonstrated in [54–56]. A multilayered printed circuit

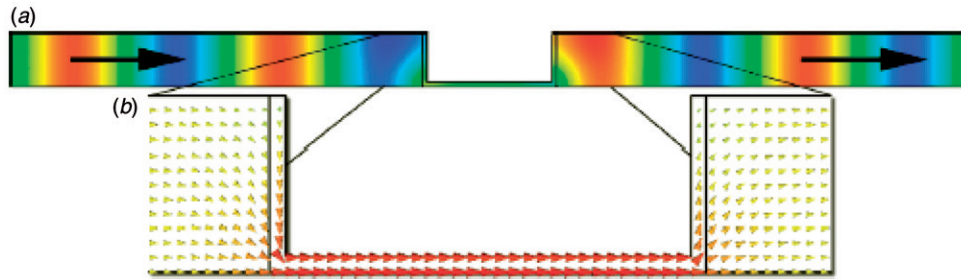


Figure 9. (a) Distribution of the normal component of magnetic field showing nearly uniform phase between the two reference planes and total transmission through an ultranarrow epsilon near zero (ENZ) channel. (b) Simulation plot of the real part of the Poynting vector distribution, showing energy flow constriction through the 'effective ENZ' region [55]. Reprinted figure with permission from Edwards et al., *Phys. Rev. Lett.* 2008, 100, 033903. Copyright (2008) by the American Physical Society. (The colour version of this figure is included in the online version of the journal.)

based on complementary split-ring resonators to produce the resonant electric response and achieve the effective zero permittivity near the plasma frequency was demonstrated in [54] (see Figure 9). In [55], the ENZ medium was constructed by a waveguide operating close to cutoff. The same principle has been realised in [55], where the ENZ channel consists of a planar waveguide in which complementary split-ring resonators are patterned on the lower surface. Realisation of a non-resonant material with extremely large index of refraction at microwaves has been demonstrated in [57] using an array of crossed metallic wires.

## 5. Superlenses

In 2000, Pendry suggested that a slab of material with negative index of refraction can act as a 'perfect lens', restoring subwavelength details by means of enhancing the evanescent fields [58]. This theoretical prediction has attracted significant interest as it offered a method for overcoming the diffraction limit in near field lenses. Recent comprehensive reviews on superlenses can be found in [25,59].

The first demonstration of focusing using a planar metamaterial slab was realised in the microwave, using a two-dimensional network of lumped inductors and capacitors [13]. A similar structure was reported to produce an image below the diffraction limit (at  $\lambda/5$ ) at approximately 1 GHz in [60]. A variant topology based on the fully uniplanar coplanar strip transmission line suitably loaded with lumped inductors and capacitors was recently employed to demonstrate free-space subwavelength near field imaging at around 2 GHz [61]. An alternative realisation in the microwave regime involved wires and split-ring resonators forming a two-dimensional waveguide and produced a focused image [62].

When the scale of the distance between the slab and both the object and its image, as well as the slab's thickness, is deeply subwavelength, the electrostatic limit can be applied. In this case, the electric and magnetic responses of a material decouple, and only one material property, namely either the electric permittivity  $\epsilon$  or the magnetic permeability  $\mu$ , needs to be negative to produce a superlens effect for transverse magnetic or transverse electric polarisation [58]. An arrangement of swiss rolls exhibiting an effective magnetic permeability of  $\mu = -1$  was demonstrated to image with a resolution of approximately  $\lambda/64$  at about 25 MHz and distance 120 mm [63]. A magnetoinductive planar lens consisting of broadside coupled split-ring resonators was demonstrated in [64] to focus a spot an order of magnitude smaller than the free space wavelength of the incoming field.

Since metals at the UV or visible frequencies exhibit an effective negative permittivity, this observation paved the way for the use of subwavelength metal sheets to obtain near-field focusing for TM polarised light. An experimental demonstration involved a 35 nm slab of silver to image objects placed 40 nm away on a photoresist under ultraviolet illumination at 365 nm and achieved resolution of 60 nm ( $\lambda/6$ ) [65]. Independently, Melville and Blaikie [66] also produced subwavelength features by virtue of a thin metal sheet. By replacing the silver with silicon carbide, which provides a better performance in terms of losses, Taubner et al. [67] achieved improved resolution of  $\lambda/20$  using the optical phonon resonance enhancement. A different experiment reports that an array of quasicrystal nanoholes in a metal screen can image a point source a few tens of wavelengths from the array into a spot on the other side of the array [68].

All the superlenses described above are in a sense near field transferring devices, as they are only capable of projecting a subwavelength image in the near field. Since the subwavelength information is coded in the

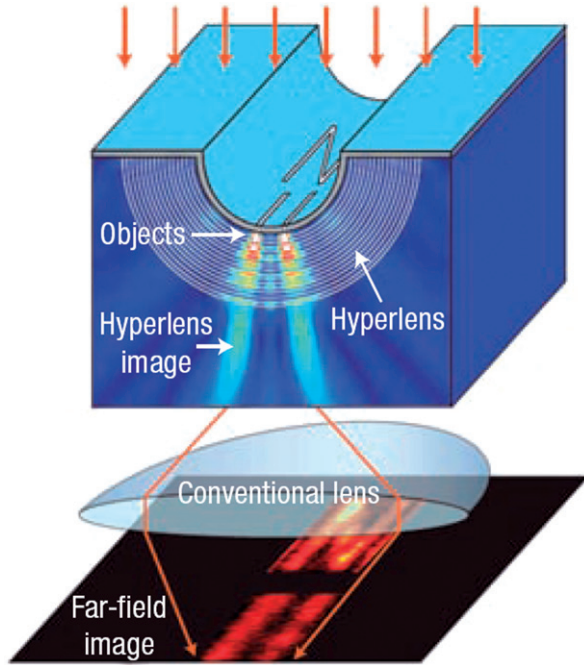


Figure 10. Schematic representation of the first far-field hyperlens experiment [73]. Reprinted with permission from Liu et al., *Science* 2007, 315, 1686. Copyright (2007) by AAAS. (The colour version of this figure is included in the online version of the journal.)

evanescent waves, which decay exponentially away from such lenses, imaging in the far field is not directly feasible. In order to achieve far-field superlenses, the evanescent fields need to be converted into propagating waves, which can then be imaged by a conventional lens in the far field. One approach to achieve this conversion was proposed by Liu et al. [69,70], where a silver superlens was structured with additional corrugations on its top surface, so that it converts the enhanced evanescent waves into propagating ones. In conjunction with a conventional optical microscope, this system was capable to image two nanoslits of 50 nm width, separated by 70 nm when illuminated by a 377 nm wavelength.

A different approach to convert evanescent waves into propagating ones was independently proposed by Jacob et al. [71], and Salandrino and Engheta [72] and involves anisotropic metamaterial with hyperbolic dispersion, which can provide magnification in a cylindrical geometry. Evanescent waves entering such an anisotropic medium become propagating and, significantly, their large transverse wavevectors are gradually compressed as they propagate outwards. If the waves propagate long enough in such a cylindrical anisotropic lens, they can eventually become propagating in air or the surrounding dielectrics. Because of the hyperbolic function associated with the dispersion in such a metamaterial, this lens is termed hyperlens.

The first optical hyperlens was reported in [73] (see Figure 10). Quartz molded with a cylindrical cavity was used as a substrate on which 16 alternating films of 35 nm silver (Ag) and 35 nm  $\text{Al}_2\text{O}_3$  were conformally deposited. Combining this hyperlens with a conventional optical microscope, an image with 130 nm resolution was directly observed in the far field for a system at wavelength 365 nm, limited by diffraction at 260 nm. A variant experiment was based on two-dimensional surface plasmon waves. The hyperlens in this case was a concentric polymer grating on a metal surface and was employed in conjunction with a conventional optical microscope [74,75].

## 6. Cloaking

Electromagnetic cloaking using metamaterials is based on the concept that a metamaterial can be used to render a volume effectively invisible to incident radiation. The design process for the cloak involves a coordinate transformation that squeezes space from a volume into a shell surrounding the concealed volume, so that the concealed volume plus the cloak appear to have the properties of free space when viewed externally; the cloak neither scatters waves nor imparts a shadow in the transmitted field [76]. The first practical realisation of such an electromagnetic cloak was reported in [76], where a copper cylinder was ‘hidden’ inside a cloak constructed by quasi-periodic resonant metallic split-ring resonator inclusions. The cloak in [76] was demonstrated for a particular polarisation at microwave frequencies (8.5 GHz). By tuning the geometric parameters of split-ring resonators, the authors were able to obtain decreased scattering from the hidden object while at the same time reducing its shadow, so that the cloak and object combined began to resemble empty space. Due to the resonant operation of the employed metamaterial, the cloak operated over a narrow band.

A similar experimental setup based on a circular cylinder annulus that behaves as an approximate cloak (nonzero scattered and nonzero interior fields) at optical frequencies was reported in [77]. The cloak in [77] was based on plasmonic nonmagnetic metamaterials producing reduced visibility at 500 nm [77]. Layers of polymethylmethacrylate (PMMA) deposited on a gold film surface were employed, so that stripes of PMMA separated by uncoated regions containing gold–air interfaces were formed.

A variant cloaking design involves a perturbation on a flat conducting plane, under which an object can be hidden [78,79] (see Figure 11). In this case an object that is placed under a curved reflecting surface is concealed by imitating the reflection of a flat surface.

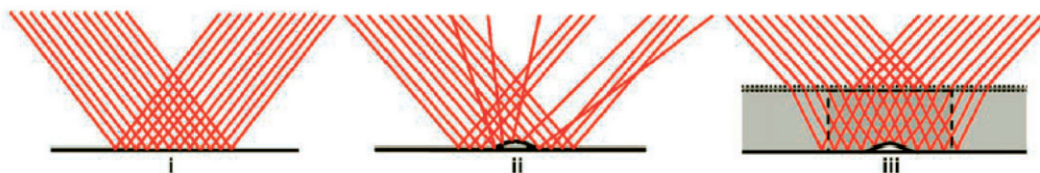


Figure 11. Ray tracing of a beam incidents illuminating on (i) a conducting ground plane, (ii) the ground plane with perturbation, and (iii) the perturbation covered by a ground-plane cloak [78]. Reprinted with permission from Liu et al., *Science* 2009, 323, 366–369. Copyright (2009) by AAAS. (The colour version of this figure is included in the online version of the journal.)

An experimental demonstration of such a ground-plane cloak was reported in [78] for a single plane of incidence and transverse electric polarisation at microwave frequencies. The design was based on non-resonant metallic (copper) elements printed on thin (0.2026 mm) FR4 substrate. Due to the non-resonant nature of this cloak, the operation bandwidth is broadband, measured by the authors between 13 and 16 GHz, and exhibits very low loss.

The proposed ground-plane cloak is suitable for scaling towards optical frequencies [78,79]. The first experimental demonstration of such an optical ‘carpet’ cloak was reported in [79]. A dielectric carpet cloak was fabricated in a 250 nm thick silicon (Si) slab waveguide. The cloak region was obtained by milling holes of constant diameter (110 nm) through the Si layer, thus varying the effective index of refraction. The design is isotropic in two dimensions. Moreover, the non-resonant operation allows for low-loss and broadband operation. The 2D implementation was demonstrated in the wavelength range of 1400 to 1800 nm.

Specially designed tapered waveguides have been shown to emulate metamaterial devices requiring anisotropic dielectric permittivity and magnetic permeability [80]. By filling a specifically shaped waveguide with an anisotropic dielectric, independent control over the effective magnetic and electric properties domain can be achieved across a broad band and with low loss. In this manner, partial two-dimensional waveguide cloaking in the visible frequency has been demonstrated at 515 and 488 nm, on a scale roughly 100 times larger than that of the incident wavelength [80].

## 7. Tunability

Attempts to dynamically control the frequency response of metamaterials have been partially motivated by the narrowband operation incurred by the resonant nature of metamaterial realisations. Other implementations have targeted to modulate incoming

radiation using dynamically tuned notch filters [81]. A series of techniques have been employed to tune metamaterial arrays in microwaves, including varactor diodes [82], photoexcitation of carriers in an amorphous space [83] and exploiting the properties of nematic liquid crystals [84–86]. In the following we focus on some recent efforts to produce tunable metamaterials at infrared and optical frequencies.

In [87] a THz metamaterial device consisting of an array of gold electric resonator elements on a semiconductor substrate (1  $\mu\text{m}$  of n-type GaAs) has been reported. The array design is based on double SRRs connected on the split gap side. The interface of the array with the substrate forms a Schottky diode and the structure has been designed to enable voltage control of the conductivity of the substrate at the split gaps. The array elements were electrically connected using conducting wires, in order for the entire array to function as a voltage gate. By applying a bias voltage, the transmission of linearly polarised normally incident plane waves has been modulated by 50% at 720 GHz. Variant geometries of the combined array/biasing structure that reduce the equivalent array resistance or capacitance have been demonstrated to improve the modulation to frequencies over 100 MHz [88].

A variant structure consisting of a doubly periodic Jerusalem cross array where each row is electrically connected with metallic wires has been demonstrated to perform as a THz phase shifter [81]. The metallic elements of the array lay on an n-doped GaAs substrate forming a Schottky diode as described above. By reverse biasing this diode, an increase in depletion occurs, which controls the transmission of linearly polarised normally incident plane waves at 810 GHz corresponding to the resonance of the array. At the slightly higher frequency of 860 GHz, the amplitude of the transmission is constant at 60% (within 10%) for different biasing voltages. However, the transmission phase was demonstrated to vary by 0.56 rad for bias voltage between 4 and 16 V [81], producing a THz phase shifter.

Optically based tunability has also been demonstrated where rather than voltage bias, the excitation of

free charge carriers in the semiconducting substrate was achieved by optical pumping [89]. A planar array of SRRs was fabricated from 3  $\mu\text{m}$  thick copper on a 670  $\mu\text{m}$  thick high resistivity gallium arsenide (GaAs) substrate. Optical pulses of 50 fs at 800 nm timed to arrive 5 ps before the peak of the THz waveform were employed to excite the carriers across the 1.42 eV band gap in GaAs. This has been demonstrated to shunt the metamaterial resonance and modify the transmission of a linearly polarised normally incident plane wave at 500 GHz by more than 70%. Improvement in switching time was reported in [90] for optically excited devices fabricated on ErAs/GaAs nano-island superlattice substrates. The fast carrier recombination in the ErAs/GaAs superlattice substrates resulted in a switching recovery time of 20 ps [90].

Photoexcitation of a silicon substrate has also been employed to produce frequency agile THz metamaterials [91]. A periodic array comprising of variants of split-ring resonators was fabricated in gold on a 530  $\mu\text{m}$  sapphire substrate. Silicon patches were realised on the other side of the substrate, forming capacitor plates at the open ends of the split-ring resonators. Optical pumping of the device by 30 fs pulses with a centre wavelength at 800 nm excited the charge carriers across the 1.12 eV band gap of silicon. By changing the conductivity of the silicon, and hence effective capacitance, tunability in the transmission of linearly polarised normally incident waves by up to 20% was experimentally demonstrated.

By adding drops of silicon nanospheres/ethanol solution to the surface of the sample near the split-ring elements, Driscoll et al. [92] demonstrated a process for tuning the magnetic resonance of a fixed SRR array. Gold split-ring resonators were patterned on a 1 mm thick silicon substrate coated with a thin 6  $\mu\text{m}$  layer of benzocyclobutane, so that the magnetic resonance of the standalone array occurs at 1.2 THz. Passive tuning was subsequently accomplished by adding dielectric material to alter the capacitance of the split-ring resonators. Droplets of 30  $\mu\text{l}$  of 0.2% solution of silicon nanospheres with 50 nm diameter suspended in ethanol were applied on the array and the sample was subsequently heated to 60°C in order to evaporate the ethanol. Repeated applications of such drops deposited additional silicon nanospheres, decreasing the resonance in steps of about 50 GHz. It is reported in [92] that the addition of silicon nanospheres does not significantly increase the thermal losses. Moreover by submerging the sample for about 30 s in an ultrasonically agitated ethanol bath, most of the silicon is removed and the resonance returns to nearly its original frequency.

An alternative approach involves thermally controlled metamaterials and is based on the variation of

the refractive index of nematic liquid crystals via phase transitions incurred by the ambient temperature [93]. The experiment reported in [93] is based on coupled metallic nanostrips covered with aligned nematic liquid crystals. By varying the ambient temperature within the range 20°C to 50°C, the magnetic response of the sample shifts from a wavelength of 650 to 632 nm. The magnetic response wavelength of the metamaterial is effectively tuned through control of the ambient temperature.

### 7.1. Active metamaterials

In order to compensate the thermal losses in photonic metamaterials, Plum et al. [94] reported functionalised complementary arrays of asymmetrical split-ring resonators with semiconductor quantum dots. The quantum dots, with the emission peak at 1050 nm, were deposited on the metamaterial array as a suspension in toluene and then dried. Upon deposition of the dots, a red shift of the transmission spectrum from 860 to 1000 nm was observed, which was attributed to increased effective permittivity of the dielectric environment. In addition, broadening of the resonance from about 70 to 105 nm was observed and attributed to the additional resonant absorption losses by the QDs. Subsequently the dots were optically pumped at 532 nm with intensities of up to 50  $\text{W cm}^{-2}$  using a frequency doubled continuous wave YAG laser. Optical pumping of the quantum dots lead to a pronounced modification of the metamaterial's transmission spectrum at the trapped-mode resonance, occurring on the background of the dots' luminescence. By comparing the pump induced change of the differential transmission signal for two perpendicular polarisations, the authors concluded that metamaterial specific to gain occurs and attributed this to strong interaction between the pumped quantum dot film and surface plasmon modes excited on the metamaterial surface.

## 8. Metasurfaces

Surfaces with tailored surface reactance, leading to prescribed boundary conditions, based on the 'fakir's bed of nails' were proposed in [95]. Theoretical and experimental results [96] implied control over the guiding, radiating and scattering properties of such surfaces, with prescribed field distributions and radiation patterns. A metallic electromagnetic structure that is characterised by having high surface impedance was proposed in [9]. The structure consists of metallic patches printed on a grounded dielectric substrate and connected to the ground with metallic vias. This surface has been demonstrated to produce in-phase

full reflection of incident plane waves and suppression of all propagating surface (and possibly leaky) waves. Reflecting the duality of the former property to that of the Perfect Electric Conductors, these surfaces have also been termed Artificial Magnetic Conductors and more recently Magnetic Mirrors [97,98]. Variations of these surfaces that omit the grounding vias have been demonstrated, suitable for easier manufacture and scaling to higher frequencies [97,99]. These structures resemble Frequency Selective Surfaces [100] printed on grounded dielectric substrates and planar reflectarrays [101].

An optical structure that reflects normally incident linearly polarised beams with wavelength in the range of 550 to 760 nm with a near zero phase has been reported in [98]. The structure consisted of a planar fishscale of 50 nm thick aluminum nanowires patterned on 50 nm of silicon dioxide and supported by a flat 150 nm aluminum mirror.

An emerging application of metamaterial surfaces is their use in planar electromagnetic absorbers. In [102], a metamaterial-based flat absorber was experimentally demonstrated at around 11.5 GHz. The design was scaled to about 1.2 THz in [103], where absorption of 70% at 1.3 THz is reported. A variant design with a more stable angular response is reported in [104], exhibiting absorption of 0.97 at 1.6 THz. In all the above, absorption occurs for a specific linear polarisation. More recently, an absorber which is nearly insensitive to the polarisation of the incoming beam was reported in [105] to produce absorption of 77% at 1.145 THz.

### 9. Metamaterials for medical imaging

The potential of metamaterial technology in applied engineering has been evident since the early days of the field. The possibility to localise electromagnetic fields beyond the diffraction limit opens up new possibilities for subwavelength sensing (imaging) and curing. For example, photolithography at the nanoscale, data storage as well as imaging and hyperthermia systems are among the applications that could benefit from metamaterials. An application that stands out for its social impact is in the field of medical imaging. In this section we report some recent experimental demonstrations of RF metamaterials in medical imaging systems and in particular in Magnetic Resonance Imaging (MRI).

The first experimental demonstration of a practical metamaterial in an MRI system was reported as early as 2001 [106]. A Marconi Medical Systems (Cleveland, Ohio) Apollo 0.5 T MRI machine operating at 21.3 MHz was used. The experiment involved an object to be

imaged (one of the author's thumbs) at a distance of 200 mm from a 10 mm thick water phantom (used to provide a reference plane), adjacent to which was located a receiver coil. When the 200 mm gap was filled with an inert plastic block, only the water phantom was visible, while all the image of the object was lost. The authors then filled this gap with a metamaterial consisting of swiss rolls of height 200 mm. The metamaterial was designed so that at the frequency of the exciting RF pulses (about 21.3 MHz) would produce a maximum magnetic permeability of  $\mu = 2.23$ . Repeating the same experiment in this case, the authors managed to image the object in good agreement with a reference measurement that they repeated using the coils integrated in the MRI machine.

A similar experimental demonstration involving a wire medium metamaterial was reported in [107]. A 3 tesla Siemens<sup>®</sup> MRI scanner was used that operates at 123.243 MHz. A wire medium was designed with the spacing between the wires equal to  $\lambda/243$  at the operating frequency and total length slightly longer than  $\lambda/2$ , in order to achieve the Fabry–Pérot matching condition. The object to be imaged was placed in the MRI magnet and the detector coil was located at the other end of the wire medium. Despite the experimental tolerances and the fact that the wire medium only transmits TM waves (hence the experiment has an inherent 3 dB loss), the authors demonstrated imaging of both a clear object (bottle of water) and a more detailed object (one of the author's hands).

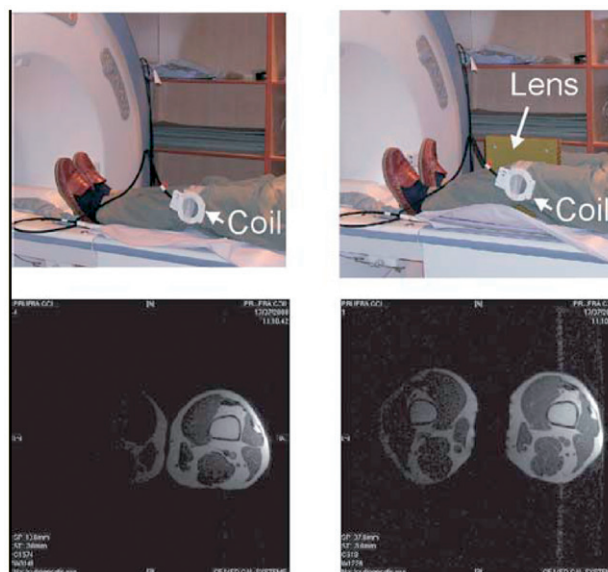


Figure 12. Image of the knees of one of the authors without the lens (left-hand side) and with the lens between the knees (right-hand side) [108]. Reprinted with permission from Freire et al., *Appl. Phys. Lett.* 2008, 93, 231108. Copyright (2008) by the American Institute of Physics. (The colour version of this figure is included in the online version of the journal.)

A variant experiment is reported in [108], where a metamaterial is used to extend the range of MRI by a single coil. The experimental setup is shown in Figure 12 and involved a General Electric 1.5 T MRI machine operating at 63.85 MHz. A magnetoinductive metamaterial consisting of copper loops loaded with nonmagnetic capacitors (from the series ATC100B specially designed by American Technical Ceramics Corp., NY, USA) was designed to produce an effective magnetic permeability of  $\mu = -1$  at the operating frequency and therefore acts as a near field superlens. A surface coil acting as a receiver was placed on the side of the left-hand side of an author's knee and two experiments were repeated with and without the metamaterial slab between the two knees (Figure 12). As shown in the result reproduced in Figure 12, both knees are imaged when the metamaterial lens is included, while the right-hand side knee is increasingly fading away from the coil in the absence of the lens. The lens refocuses the signal emitted from the right-hand side knee, which can then be picked up by the coil, extending the imaging range of the surface coil.

## 10. Outlook

The beginning of the field of metamaterials can be placed about 10 years ago, with Pendry's suggestion of the possibility for engineered composites with magnetic response [10]. Since then, metamaterials represent a rapidly growing area of research which calls for expertise across several branches of physics, engineering and mathematics. Although the scattering and propagation of electromagnetic fields in periodic structures has been studied for many decades [109,110], the collective, consistent and coordinated activity that was initiated within the field of metamaterials has produced a significant volume of theoretical and experimental results. The progress achieved since the first experimental demonstration of metamaterials has been striking. Since the experiment reported in [12], metamaterials have been brought from microwave to optical frequencies. New and exciting proof-of-concept demonstrations such as subwavelength imaging and cloaking have been achieved adding extra momentum to the field. However, to functionalise metamaterials into practical applications there are still as many remaining goals to be achieved, including for example the realisation of isotropic three-dimensional composites with reduction of losses that operate over a broad bandwidth and which further are dynamically controlled. The recent remarkable achievements and the remaining big challenges promise exciting developments within the area of metamaterials in the future.

## References

- [1] Kock, W.E. *Proceedings, IRE and Waves and Electrons* **1946**, *34*, 828–836, November.
- [2] Stuetzer, O.M. *Proc. IRE* **1950**, *38*, 1053–1056.
- [3] Corkum, R.W. *Proc. IRE* **1952**, *40*, 574–587.
- [4] Ward, H.T.; Puro, W.O.; Bowie, D.M. *Proc. IRE* **1956**, *44*, 171–174.
- [5] Kolettis, N.J.; Collin, R.E. *IRE Trans. Microwave Theory Tech.* **1961**, *9*, 436–441.
- [6] Rotman, W. *IRE Trans. Antennas Propagat.* **1962**, *10*, 82–95.
- [7] Golden, K. *IEEE Trans. Antennas Propagat.* **1965**, *13*, 587–594.
- [8] Yablonovitch, E. *Phys. Rev. Lett.* **1987**, *58*, 2059–2062.
- [9] Sievenpiper, D.; Lijun, Z.; Broas, R.F.; Alexopoulos, N.G.; Yablonovitch, E. *IEEE Trans. Microwave Theory Tech.* **1999**, *47*, 2059–2074.
- [10] Pendry, J.B.; Holden, A.J.; Robbins, D.J.; Stewart, W.J. *IEEE Trans. Microwave Theory Tech.* **1999**, *47*, 2075–2084.
- [11] Veselago, V.G. *Sov. Phys. Usp.* **1968**, *10*, 509–514.
- [12] Shelby, R.A.; Smith, D.R.; Schultz, S. *Science* **2001**, *292*, 77.
- [13] Eleftheriades, G.V.; Iyer, A.K.; Kremer, P.C. *IEEE Trans. Microwave Theory Tech.* **2002**, *50*, 2702.
- [14] Sanada, A.; Caloz, C.; Itoh, T. *IEEE Trans. Microwave Theory Tech.* **2004**, *52*, 1252.
- [15] Yen, T.J.; Padilla, W.J.; Fang, N.; Vier, D.C.; Smith, D.R.; Pendry, J.B.; Basov, D.N.; Zhang, X. *Science* **2004**, *303*, 1494–1496.
- [16] Linden, S.; Enkrich, C.; Wegener, M.; Zhou, J.; Koschny, T.; Soukoulis, C.M. *Science* **2004**, *306*, 1351–1353.
- [17] Enkrich, C.; Wegener, M.; Linden, S.; Burger, S.; Zschiedrich, L.; Schmidt, F.; Zhou, J.F.; Koschny, T.; Soukoulis, C.M. *Phys. Rev. Lett.* **2005**, *95*, 203901–203904.
- [18] Zhang, S.; Fan, W.; Minhas, B.K.; Frauenglass, A.; Malloy, K.J.; Brueck, S.R.J. *Phys. Rev. Lett.* **2005**, *94*, 37402–37404.
- [19] Katsarakis, N.; Konstantinidis, G.; Kostopoulos, A.; Penciu, R.S.; Gundogdu, T.F.; Kafesaki, M.; Economou, E.N.; Koschny, Th.; Soukoulis, C.M. *Opt. Lett.* **2005**, *30*, 1348–1350.
- [20] Zhou, J.F.; Koschny, T.; Kafesaki, M.; Economou, E.N.; Pendry, J.B.; Soukoulis, C.M. *Phys. Rev. Lett.* **2005**, *95*, 223902.
- [21] Klein, M.W.; Enkrich, C.; Wegener, M.; Soukoulis, C.M.; Linden, S. *Opt. Lett.* **2005**, *31*, 1259–1261.
- [22] Podolskiy, V.A.; Sarychev, A.K.; Shalaev, V.M. *J. Nonlinear Opt. Phys. Mater.* **2002**, *11*, 65–74.
- [23] Yuan, H.K.; Chettiar, U.K.; Cai, W.; Kildishev, A.V.; Boltasseva, A.; Drachev, V.P.; Shalaev, V.M. *Opt. Express* **2007**, *15*, 1076.
- [24] Cai, W.; Chettiar, U.K.; Yuan, H.-K.; de Silva, V.C.; Kildishev, A.V.; Drachev, V.P.; Shalaev, V.M. *Opt. Express* **2007**, *15*, 3333–3341.
- [25] Eleftheriades, G. *Material Today* **2009**, *12*, 30–41.

- [26] Soukoulis, C.M.; Zhou, J.; Koschny, T.; Kafesaki, M.; Economou, E.N. *J. Phys.: Condens. Matter* **2008**, *20*, 304217.
- [27] Chettiar, U.K.; Xiao, S.; Kildishev, A.V.; Cai, W.; Yuan, H.-K.; Drachev, V.P.; Shalaev, V.M. *MRS Bull.* **2008**, *38*, 921–926.
- [28] Boltasseva, A.; Shalaev, V.M. *Metamaterials* **2008**, *2*, 1–17.
- [29] Zhou, J.; Zhang, L.; Tuttle, G.; Koschny, T.; Soukoulis, C.M. *Phys. Rev. B* **2006**, *73*, 041101.
- [30] Zhou, J.; Koschny, T.; Zhang, L.; Tuttle, G.; Soukoulis, C.M. *Appl. Phys. Lett.* **2006**, *88*, 221103.
- [31] Liu, R.; Degiron, A.; Mock, J.J.; Smith, D.R. *Appl. Phys. Lett.* **2007**, *90*, 263504.
- [32] Gokkavas, M.; Guven, K.; Bulu, I.; Aydin, K.; Penciu, R.S.; Kafesaki, M.; Soukoulis, C.M.; Ozbay, E. *Phys. Rev. B* **2006**, *73*, 193103.
- [33] Litchinitser, N.M.; Shalaev, V.M. *Laser Phys. Lett.* **2008**, *5*, 411–420.
- [34] Shalaev, V.M.; Cai, W.; Chettiar, U.K.; Yuan, H.-K.; Sarychev, A.K.; Drachev, V.P.; Kildishev, A.V. *Opt. Lett.* **2005**, *30*, 3356.
- [35] Dolling, G.; Enkrich, C.; Wegener, M.; Zhou, J.F.; Soukoulis, C.M.; Linden, S. *Opt. Lett.* **2005**, *30*, 3198.
- [36] Soukoulis, C.M.; Linden, S.; Wegener, M. *Science* **2007**, *315*, 47–49.
- [37] Zhang, S.; Fan, W.; Panoiu, N.C.; Malloy, K.J.; Osgood, R.M.; Brueck, S.R.J. *Phys. Rev. Lett.* **2005**, *95*, 137404.
- [38] Dolling, G.; Enkrich, C.; Wegener, M.; Soukoulis, C.M.; Linden, S. *Opt. Lett.* **2006**, *31*, 1800–1802.
- [39] Dolling, G.; Enkrich, C.; Wegener, M.; Soukoulis, C.M.; Linden, S. *Science* **2006**, *32*, 892–894.
- [40] Dolling, G.; Wegener, M.; Soukoulis, C.M.; Linden, S. *Opt. Lett.* **2007**, *32*, 53–55.
- [41] Chettiar, U.K.; Kildishev, A.V.; Yuan, H.-K.; Cai, W.; Xiao, S.; Drachev, V.P.; Shalaev, V.M. *Opt. Lett.* **2007**, *32*, 1671–1673.
- [42] Valentine, J.; Zhang, S.; Zentgraf, T.; Ulin-Avila, E.; Genov, D.A.; Bartal, G.; Zhang, X. *Nature* **2008**, *455*, 376–379.
- [43] Tretyakov, S.; Nefedov, I.; Sihvola, A.; Maslovski, S.; Simovski, C. *J. Electromagn. Waves. Appl.* **2003**, *17*, 695.
- [44] Pendry, J.B. *Science* **2004**, *306*, 1353.
- [45] Monzon, C.; Forester, D.W. *Phys. Rev. Lett.* **2005**, *95*, 123904.
- [46] Rogacheva, A.V.; Fedotov, V.A.; Schwanecke, A.S.; Zheludev, N.I. *Phys. Rev. Lett.* **2006**, *97*, 77401.
- [47] Plum, E.; Zhou, J.; Dong, J.; Fedotov, V.A.; Koschny, T.; Soukoulis, C.M.; Zheludev, N.I. *Phys. Rev. B* **2009**, *79*, 035407.
- [48] Zhang, S.; Park, Y.-S.; Li, J.; Lu, X.; Zhang, W.; Zhang, X. *Phys. Rev. Lett.* **2009**, *102*, 023901.
- [49] Wiltshire, M.C.K.; Hajnal, J.V.; Pendry, J.B.; Edwards, D.J. *Opt. Express* **2003**, *11*, 709–715.
- [50] Belov, P.A.; Hao, Y.; Sudhakaran, S. *Phys. Rev. B* **2006**, *73*, 033108.
- [51] Belov, P.A.; Zhao, Y.; Tse, S.; Ikonen, P.; Silveirinha, M.G.; Simovski, C.R.; Tretyakov, S.; Hao, Y.; Parini, C. *Phys. Rev. B* **2008**, *77*, 193108.
- [52] Yao, J.; Liu, Z.; Liu, Y.; Wang, Y.; Sun, C.; Bartal, G.; Stacy, A.; Zhang, X. *Science* **2008**, *321*, 930.
- [53] Dolling, G.; Wegener, M.; Linden, S. *Opt. Lett.* **2007**, *32*, 551–553.
- [54] Cheng, Q.; Liu, R.; Huang, D.; Cuia, T.J.; Smith, D.R. *Appl. Phys. Lett.* **2007**, *91*, 234105.
- [55] Edwards, B.; Alu, A.; Young, M.E.; Silveirinha, M.; Engheta, N. *Phys. Rev. Lett.* **2008**, *100*, 033903.
- [56] Liu, R.; Cheng, Q.; Hand, T.; Mock, J.J.; Cui, T.J.; Cummer, S.A.; Smith, D.R. *Phys. Rev. Lett.* **2008**, *100*, 023903.
- [57] Silveirinha, M.G.; Fernandes, C.A.; Costa, J.R.; Medeiros, C.R. *Appl. Phys. Lett.* **2008**, *93*, 174103.
- [58] Pendry, J.B. *Phys. Rev. Lett.* **2000**, *85*, 3966–3969.
- [59] Ziang, X.; Liu, Z. *Nature* **2008**, *7*, 436–441.
- [60] Grbic, A.; Eleftheriades, G.V. *Phys. Rev. Lett.* **2004**, *92*, 117403.
- [61] Iyer, A.K.; Eleftheriades, G.V. *IEEE Trans. Antennas Propagat.* **2009**, *57*, 1720–1727.
- [62] Houck, A.A.; Brock, J.B.; Chuang, I.L. *Phys. Rev. Lett.* **2003**, *90*, 137401.
- [63] Wiltshire, M.C.K.; Pendry, J.B.; Hajnal, J.V. *J. Phys.: Condens. Matter* **2006**, *18*, L315–L321.
- [64] Freirea, M.J.; Marqués, R. *Appl. Phys. Lett.* **2005**, *86*, 182505.
- [65] Fang, N.; Lee, H.; Sun, C.; Ziang, X. *Science* **2005**, *308*, 534–537.
- [66] Melville, D.; Blaikie, R. *Opt. Express* **2005**, *13*, 2127–2134.
- [67] Taubner, T.; Korobkin, D.; Urzhumov, Y.; Shvets, G.; Hillenbrand, R. *Science* **2006**, *313*, 1595.
- [68] Huang, F.M.; Kao, T.S.; Fedotov, V.A.; Chen, Y.; Zheludev, N.I. *Nano Lett.* **2008**, *8*, 2469–2472.
- [69] Liu, Z.; Durant, S.; Lee, H.; Pikus, Y.; Fang, N.; Xiong, Y.; Sun, C.; Zhang, X. *Nano Lett.* **2007**, *7*, 403–408.
- [70] Liu, Z.; Durant, S.; Lee, H.; Pikus, Y.; Xiong, Y.; Sun, C.; Zhang, X. *Opt. Express* **2007**, *15*, 6947–6954.
- [71] Jacob, Z.; Alekseyev, L.V.; Narimanov, E. *Opt. Express* **2006**, *14*, 8247–8256.
- [72] Salandrino, A.; Engheta, N. *Phys. Rev. B* **2006**, *74*, 075103.
- [73] Liu, Z.; Lee, H.; Xiong, Y.; Sun, C.; Zhang, X. *Science* **2007**, *315*, 1686.
- [74] Smolyaninov, I.I.; Huang, Y.J.; Davis, C.C. *Science* **2007**, *315*, 1699–1701.
- [75] Drezet, A.; Hohenau, A.; Krenn, J.R. *Phys. Rev. Lett.* **2007**, *98*, 209730.
- [76] Schurig, D.; Mock, J.J.; Justice, B.J.; Cummer, S.A.; Pendry, J.B.; Starr, A.F.; Smith, D.R. *Science* **2006**, *314*, 977–980.
- [77] Smolyaninov, I.I.; Hung, Y.J.; Davis, C.C. *Opt. Lett.* **2008**, *33*, 1342–1344.
- [78] Liu, R.; Ji, C.; Mock, J.J.; Chin, J.Y.; Cui, T.J.; Smith, D.R. *Science* **2009**, *323*, 366–369.
- [79] Valentine, J.; Li, J.; Zentgraf, T.; Bartal, G.; Zhang, X. *Nature Materials* **2009**, *8*, 568–571.
- [80] Smolyaninov, I.I.; Smolyaninova, V.N.; Kildishev, A.V.; Shalaev, V.M. *Phys. Rev. Lett.* **2009**, *102*, 213901-4.

- [81] Chen, H.-T.; Padilla, W.J.; Cich, M.J.; Azad, A.K.; Averitt, R.D.; Taylor, A.J. *Nature Photonics* **2009**, *3*, 148–151.
- [82] Mias, C.; Yap, J.H. *IEEE Trans. Antennas Propagat.* **2007**, *55*, 1955–1962.
- [83] Kim, E.; Shen, Y.R.; Wu, W.; Poinzovskaya, E.; Yu, Z.; Bratkovsky, A.M.; Wand, S.Y.; Williams, R.S. *Appl. Phys. Lett.* **2007**, *91*, 173105.
- [84] Werner, D.H.; Kwon, D.-H.; Khoo, I.-C.; Kildishev, A.K.; ShalaeV, V.M. *Opt. Express* **2007**, *15*, 3342.
- [85] Zhao, Q.; Kang, L.; Du, B.; Li, B.; Zhou, J.; Tang, H.; Liang, X.; Zhang, B. *Appl. Phys. Lett.* **2007**, *90*, 011112.
- [86] Zhang, F.; Zhao, Q.; Kang, L.; Gaillot, D.P.; Zhao, X.; Zhou, J. *Appl. Phys. Lett.* **2008**, *92*, 193104.
- [87] Chen, H.-T.; Padilla, W.J.; Zide, J.M.O.; Gossard, A.C.; Taylor, A.J.; Averitt, R.D. *Nature* **2006**, *444*, 597–600.
- [88] Chen, H.-T.; Palit, S.; Tyler, T.; Bingham, C.M.; Zide, J.M.O.; O'Hara, J.F.; Smith, D.R.; Gossard, A.C.; Averitt, R.D.; Padilla, W.J.; Jokerst, N.M.; Taylor, A.J. *Appl. Phys. Lett.* **2008**, *93*, 091117.
- [89] Padilla, W.J.; Taylor, A.J.; Highstrete, C.; Lee, M.; Averitt, R.D. *Phys. Rev. Lett.* **2006**, *96*, 107401.
- [90] Chen, H.-T.; Padilla, W.J.; Zide, J.M.O.; Bank, S.R.; Gossard, A.C.; Taylor, A.J.; Averitt, R.D. *Opt. Lett.* **2007**, *32*, 1620–1622.
- [91] Chen, H.-T.; O'Hara, J.F.; Aazad, A.K.; Taylor, A.J.; Averitt, R.D.; Shrekenhamer, D.B.; Padilla, W.J. *Nature Photonics* **2008**, *2*, 295–298.
- [92] Driscoll, T.; Andreev, G.O.; Basov, D.N.; Palit, S.; Cho, S.Y.; Jokerst, N.M.; Smith, D.R. *Appl. Phys. Lett.* **2007**, *91*, 062511.
- [93] Xiao, S.; Chettiar, U.K.; Kildishev, A.V.; Drachev, V.; Khoo, I.C.; ShalaeV, V.M. *Appl. Phys. Lett.* **2009**, *95*, 033115.
- [94] Plum, E.; Fedotov, V.A.; Kuo, P.; Tsai, D.P.; Zheludev, N.I. *Opt. Express* **2007**, *17*, 8548–8551.
- [95] King, R.J.; Park, K.S. *Electron. Lett.* **1981**, *17*, 52–53.
- [96] King, R.; Thiel, D.; Park, K. *IEEE Trans. Antennas Propagat.* **1983**, *31*, 471–476.
- [97] Feresidis, A.; Goussetis, G.; Wang, S.; Vardaxoglou, J.C. *IEEE Trans. Antennas Propagat.* **2005**, *53*, 209–215.
- [98] Schwanecke, A.S.; Fedotov, V.A.; Khardikov, V.V.; Prosvirnin, S.L.; Chen, Y.; Zheludev, N.I. *J. Opt. A: Pure Appl. Opt.* **2007**, *9*, 1464.
- [99] Fei-Ran, Y.; Kuang-Ping, M.; Yongxi, Q.; Itoh, T. *IEEE Trans. Microwave Theory Tech.* **1999**, *47*, 1509–1514.
- [100] Munk, B. *Frequency Selective Surfaces: Theory and Design*; Wiley: New York, 2000.
- [101] Pozar, D.M.; Targonski, S.D.; Syrigos, H.D. *IEEE Trans. Antennas Propagat.* **1997**, *45*, 287–296.
- [102] Landy, N.I.; Sajuyigbe, S.; Mock, J.J.; Smith, D.R.; Padilla, W.J. *Phys. Rev. Lett.* **2008**, *100*, 207402.
- [103] Tao, H.; Landy, N.I.; Bingham, C.M.; Zhang, X.; Averitt, R.D.; Padilla, W.J. *Opt. Express* **2008**, *16*, 7181–7188.
- [104] Tao, H.; Bingham, C.M.; Strikwerda, A.C.; Pilon, D.; Shrekenhamer, D.; Landy, N.I.; Fan, K.; Zhang, X.; Padilla, W.J.; Averitt, R.D. *Phys. Rev. B* **2008**, *78*, 241103.
- [105] Landy, N.I.; Bingham, C.M.; Tyler, T.; Jokerst, N.; Smith, D.R.; Padilla, W.J. *Phys. Rev. B* **2009**, *79*, 125104.
- [106] Wiltshire, M.C.K.; Pendry, J.B.; Young, I.R.; Larkman, D.J.; Gilderdale, D.J.; Hajnal, J.V. *Science* **2001**, *291*, 849–851.
- [107] Radu, X.; Lapeyronnie, A.; Craeye, C. *Electromagnetics* **2008**, *28*, 531–543.
- [108] Freire, M.J.; Marques, R.; Jelinek, L. *Appl. Phys. Lett.* **2008**, *93*, 231108.
- [109] Spielman, B.E.; Amari, S.; Caloz, C.; Eleftheriades, G.V.; Itoh, T.; Jackson, D.R.; Levy, R.; Rhodes, J.D.; Snyder, R.V. *IEEE Microwave Mag.* **2009**, *May*, 8–42.
- [110] Munk, B. *Metamaterial: Critique and Alternatives*; Wiley: New Jersey, 2009.